Mechanisms of three-dimensional structuring of photo-polymers by tightly focussed femtosecond laser pulses

Mangirdas Malinauskas[1,3], Albertas Žukauskas[1], Gabija Bičkauskaitė[1], Roaldas Gadonas[1,4], and Saulius Juodkazis[2,*]

[1] *Laser Nanophotonics Group, Department of Quantum Electronics, Physics Faculty, Vilnius University, Saulėtekio avenue 9, bldg. III, LT-10222 Vilnius, Lithuania*
[2] *Centre for Micro-Photonics, Faculty of Engineering and Industrial Sciences, Swinburne University of Technology, Hawthorn, VIC, 3122, Australia*
[3] *mangirdas.malinauskas@ff.vu.lt*
[4] *roaldas.gadonas@ff.vu.lt*
[*] *sjuodkazis@swin.edu.au*

Abstract: Three-dimensional (3D) micro/nano-structuring of photo-resists is systematically studied at the close-to-dielectric-breakdown irradiance. It is demonstrated that avalanche absorption is playing a major part in free electron generation and chemical bond breaking at these conditions. The steps of photo-initiation and chemical bond breaking in propagation of polymerization are altered as compared with photo-polymerization at low-irradiance and one-photon stereo-lithography. The avalanche dominates radical generation and promotion of polymerization at tight focusing and a high $\sim$TW/cm^2 irradiance. The rates of electron generation by two-photon absorption and avalanche are calculated for the experimental conditions. Simulation results are corroborated by 3D polymerization in three resists with different photo-initiators at two different wavelengths and pulse durations. The smallest feature sizes of 3D polymerized logpile structures are consistent with spectral dependencies of the two photon nonlinearities. Implications of these findings for achieving sub-100 nm resolution in 3D structuring of photo-polymers are presented.

OCIS codes: (140.3390) Laser materials processing; (220.4000) Microstructure fabrication; (160.1245) Artificially engineered materials.

References and links

1. M. Farsari and B. Chichkov, "Materials processing: Two-photon fabrication," Nat. Photon. **3**, 450 – 452 (2009).
2. J. K. Gansel, K. Justyna, M. Thiel, M. S. Rill, M. Decker, K. Bade, V. Saile, G. von Freymann, S. Linden, and M. Wegener, "Gold Helix Photonic Metamaterial as Broadband Circular Polarizer," Science **325**, 1513–1515 (2009).
3. R. R. Gattass and E. Mazur, "Femtosecond laser micromachining in transparent materials," Nat. Photon. **2**, 219–222 (2008).
4. T. Tanaka, A. Ishikawa, and S. Kawata, "Two-photon-induced reduction of metal ions for fabricating three-dimensional electrically conductive metallic microstructure," Appl. Phys. Lett. **88**, 081107 (2006).
5. S. Kawata, H.-B. Sun, T. Tanaka, and K. Takada, "Finer features for functional microdevices," Nature **412**, 697–698 (2001).
6. L. Li, R. R. Gattass, E. Gershgoren, H. Hwang, and J. T. Fourkas, "Achieving $\lambda/20$ Resolution by One-Color Initiation and Deactivation of Polymerization," Science **324**, 910–913 (2009).

#125161 - $15.00 USD Received 8 Mar 2010; revised 2 Apr 2010; accepted 5 Apr 2010; published 30 Apr 2010

7. S. H. Park, T. W. Lim, D. Y. Yang, R. H. Kim, and K. S. Lee, "Improvement of spatial resolution in nano-stereolithography using radical quencher," Macromol. Res. **14**, 559–564 (2006).
8. S. K. Sundaram and E. Mazur, "Inducing and probing non-thermal transitions in semiconductors using femtosecond laser pulses," Nat. Mater. **1**, 217–224 (2002).
9. C. A. Mack, *Optical Lithography*, (SPIE Field Guides, vol. FG06, SPIE Press, Bellingham, 2006).
10. S. Maruo, O. Nakamura, and S. Kawata, "Three-dimensional microfabrication with two-photon-absorbed photopolymerization," Opt. Lett. **2**, 132 – 134 (1997).
11. R. A. Borisov, G. N. Dorojkina, N. I. Koroteev, V. M. Kozenkov, S. A. Magnitskii, D. V. Malakhov, A. V. Tarasishin, and A. M. Zheltikov, "Femtosecond two-photon photopolymerization: a method to fabricate optical photonic crystals with controllable parameters," Laser Phys. **8**, 1105–1105 (1998).
12. J. Serbin, A. Egbert, A. Ostendorf, B. N. Chichkov, R. Houbertz, G. Domann, J. Schulz, C. Cronauer, L. Frohlich, and M. Popall, "Femtosecond laser-induced two-photon polymerization of inorganic-organic hybrid materials for applications in photonics," Opt. Lett. **28**, 301–303 (2003).
13. M. Straub and M. Gu, "Near-infrared photonic crystals with higher-order bandgaps generated by two-photon photopolymerization," Opt. Lett. **27**, 1824–1826 (2002).
14. S. H. Park, S. H. Lee, D.-Y. Yang, H. J. Kong, and K.-S. Lee, "Subregional slicing method to increase three-dimensional nanofabrication efficiency in two-photon polymerization," Appl. Phys. Lett. **87**, 154108 (2005).
15. F. Qi, Y. Li, D. Tan, H. Yang, and Q. Gong, "Polymerized nanotips via two-photon photopolymerization," Opt. Express **15**, 971–976 (2007).
16. M. Malinauskas, V. Purlys, M. Rutkauskas, and R. Gadonas, "Two-photon polymerization for fabrication of three-dimensional micro- and nanostructures over a large area," in Proceedings of *Micromachining and Microfabrication Process Technology XIV* (SPIE Proc. 7204, 2009) pp. 72040C/1–11.
17. A. Pikulin and N. Bityurin, "Spatial resolution in polymerization of sample features at nanoscale," Phys. Rev. B **75**, 195430 (2009).
18. N. Uppal and P. S. Shiakolas, "Modeling of temperature-dependent diffusion and polymerization kinetics and their effects on two-photon polymerization dynamics," J. Micro/Nanolith. MEMS MOEMS **7**, 043002 (2008).
19. K. K. Seet, S. Juodkazis, V. Jarutis, and H. Misawa, "Feature-size reduction of photopolymerized structures by femtosecond optical curing of SU-8," Appl. Phys. Lett. **89**, 024106 (2006).
20. T. Baldacchini, C. N. LaFratta, R. A. Farrer, M. C. Teich, B. E. A. Saleh, M. J. Naughton, and J. T. Fourkas, "Acrylic-based resin with favorable properties for three-dimensional two-photon polymerization," J. Appl. Phys. **95**, 6072–6076 (2004).
21. H. Xia, W.-Y. Zhang, F.-F. Wang, D. Wu, X.-W. Liu, L. L. Chen, Q.-D. Chen, Y.-G. Ma, and H.-B. Sun, "Three-dimensional micronanofabrication via two-photon-excited photoisomerization," Appl. Phys. Lett. **95**, 083118 (2009).
22. R. W. Boyd, *Nonlinear Optics* (Academic Press, London, 2nd ed., 2003).
23. A. Ovsianikov, J. Viertl, B. Chichkov, M. Oubaha, B. MacCraith, I. Sakellari, A. Giakoumaki, D. Gray, M. Vamvakaki, M. Farsari, and C. Fotakis, "Ultra-low shrinkage hybrid photosensitive material for two-photon polymerization microfabrication," ACS Nano **2**, 2257–2262 (2008).
24. A. Ovsianikov, A. Gaidukeviciute, B. N. Chichkov, M. Oubaha, B. D. MacCraith, I. Sakellari, A. Giakoumaki, D. Gray, M. Vamvakaki, M. Farsari, and C. Fotakis, "Two-photon polymerization of hybrid sol-gel materials for photonics applications," Laser Chem. **2008**, ID 493059 (2008).
25. V. Mizeikis, K. K. Seet, S. Juodkazis, and H. Misawa, "Three-dimensional woodpile photonic crystal templates for infrared spectral range," Opt. Lett. **29**, 2061 – 2063 (2004).
26. A. E. Siegman, *Lasers* (University Science Books, Mill Valley, 1986).
27. M. Sheik-bahae, A.A.Said, T. H. Wei, D. J. Hagan, and E. W. van Stryland, "Sensitive measurement of optical nonlinearities using a single beam," IEEE J. Quantum Electr. **26**, 760–769 (1990).
28. K. Kamada, "Characterization of two-photon absorption and its resonance enhancement by z-scan method," in Proceedings of *Nonlinear Optical Transmission and Multiphoton Processes in Organics II*, (SPIE Proc. 5516, 2004), pp. 97–105.
29. K. Kamada, K. Matsunaga, A. Yoshino, and K. Ohta, "Two-photon-absorption-induced accumulated thermal effect on femtosecond Z-scan experiments studied with time-resolved thermal-lens spectrometry and its simulation," J. Opt. Soc. Am. B **20**, 529–537 (2003).
30. R. DeSalvo, A. A. Said, D. Hagan, E. W. VanStryland, and M. SheikBahae, "Infrared to ultraviolet measurements of two-photon absorption and n(2) in wide bandgap solids," IEEE J. Quantum Electr. **32**, 1324–1333 (1996).
31. M. Rumi, J. Ehrlich, A. Heikal, J. Perry, S. Barlow, Z. Hu, D. McCord-Maughon, T. C. Parker, H. Rockel, S.Thayumanavan, S. R. Marder, D. Beljonne, and J.-L. Bredas, "Structure-property relationships for two-photon absorbing chromophores: Bis-donor diphenylpolyene and bis(styryl)benzene derivatives," J. Am. Chem. Soc. **122**, 9500–9510 (2000).
32. N. Murazawa, S. Juodkazis, H. Misawa, and K. Kamada, "Two-photon excitation of dye-doped liquid crystal by a cw-laser irradiation," Mol. Cryst. Liq. Cryst. **489**, 310–319 (2008).
33. S. Juodkazis, V. Mizeikis, and H. Misawa, "Three-dimensional structuring of resists and resins by direct laser writing and holographic recording," Adv. Polym. Sci. **213**, 157–206 (2008).

#125161 - $15.00 USD Received 8 Mar 2010; revised 2 Apr 2010; accepted 5 Apr 2010; published 30 Apr 2010

34. H. J. Eichler, F. Massmann, E. Biselli, K. Richter, M. Glotz, L. Konetzke, and X. Yang, "Laser-induced free-carrier and temperature gratings in silicon," Phys. Rev. B **36**, 3247–3253 (1987).
35. E. Gamaly, A. Rode, B. Luther-Davies, and V. Tikhonchuk, "Ablation of solids by femtosecond lasers: Ablation mechanism and ablation thresholds for metals and dielectrics," Phys. Plasmas **9**, 949–957 (2002).
36. B. C. Stuart, M. D. Feit, S. Herman, A. M. Rubenchik, B. W. Shore, and M. D. Perry, "Nanosecond-to-femtosecond laser-induced breakdown in dielectrics," Phys. Rev. B **53**, 1749–1761 (1996).
37. Y. P. Raizer, *Laser-induced discharge phenomena* (Consultant Bureau, New York, 1977).
38. A. Vogel, J. Noack, G. Hüttman, and G. Paltauf, "Mechanisms of femtosecond laser nanosurgery of cells and tissues," Appl. Phys. B **81**, 1015–1047 (2005).
39. S. Juodkazis, A. V. Rode, E. G. Gamaly, S. Matsuo, and H. Misawa, "Recording and reading of three-dimensional optical memory in glasses," Appl. Phys. B **77**, 361–368 (2003).
40. K. Yamasaki, S. Juodkazis, T. Lippert, M. Watanabe, S. Matsuo, and H. Misawa, "Dielectric breakdown of rubber materials by femtosecond irradiation," Appl. Phys. A. **76**, 325–329 (2003).
41. S. Juodkazis, V. Mizeikis, Y. Nishijima, W. Ebina, H. Misawa, M. Kondo, and V.Švrček, "Three-dimensional femtosecond laser fabrication," ECS Transact. **16**, 57–63 (2009).
42. S. Juodkazis, V. Mizeikis, and H. Misawa, "Three-dimensional microfabrication of materials by femtosecond lasers for photonics applications," J. Appl. Phys. **106**, 051101 (2009).
43. S. Maruo and K. Ikuta, "Three-dimensional microfabrication by use of single-photon-absorbed polymerization," Appl. Phys. Lett. **76**, 2656–2658 (2000).
44. S. Juodkazis, V. Mizeikis, S. Matsuo, K. Ueno, and H. Misawa, "Three-dimensional micro- and nano-structuring of materials by tightly focused laser radiation," Bull. Chem. Soc. Jpn. **81**, 411–448 (2008).
45. J. Morikawa, A. Orie, T. Hashimoto, and S. Juodkazis, "Thermal diffusivity in femtosecond-laser-structured micro-volumes of polymers," Appl. Phys. A. **98**, 551–556 (2010).
46. K. Ueno, S. Juodkazis, T. Shibuya, V. Mizeikis, Y. Yokota, and H. Misawa, "Nano-particle-enhanced photo-polymerization," J. Phys. Chem. C **113**, 11720–11724 (2009).
47. S. Juodkazis, V. Mizeikis, K. K. Seet, H. Misawa, and U. G. K. Wegst, "Mechanical properties and tuning of three-dimensional polymeric photonic crystals," Appl. Phys. Lett. **91**, 241904 (2007).
48. Q. Sun, S. Juodkazis, N. Murazawa, V. Mizeikis, and H. Misawa, "Freestanding and movable photonic microstructures fabricated by photopolymerization with femtosecond laser pulses," J. Micromech. Microeng. **20**, 035004/1–5 (2010).
49. A. Benayas, D. Jaque, B. McMillen, and K. P. Chen, "High repetition rate UV ultrafast laser inscription of buried channel waveguides in sapphire: Fabrication and fluorescence imaging via ruby R lines," Opt. Express **17**, 10076–10081 (2009).
50. K. Sugioka, Y. Cheng, and K. Midorikawa, "Three-dimensional micromachining of glass using femtosecond laser for lab-on-a-chip device manufacture," Appl. Phys. A **81**, 1–10 (2005).
51. G. Cerullo, R. Osellame, S. Taccheo, M. Marangoni, D. Polli, R. Ramponi, P. Laporta, and S. D. Silvestri, "Femtosecond micromachining of symmetric waveguides at 1.5μm by astigmatic beam focusing," Opt. Lett. **27**, 1938–1940 (2002).
52. G. Cheng, K. Mishchik, C. Mauclair, E. Audouard, and R. Stoian, "Ultrafast laser photoinscription of polarization sensitive devices in bulk silica glass," Opt. Express **17**, 9515–9525 (2009).
53. D. Day and M. Gu, "Microchannel fabrication in PMMA based on localized heating by nanojoule high repetition rate femtosecond pulses," Opt. Express **13**, 5939–5946 (2005).
54. S. Nolte, M. Will, J. Burghoff, and A. Tünnermann, "Femtosecond waveguide writing: a new avenue to three-dimensional integrated optics," Appl. Phys. A **77**, 109–111 (2003).
55. L. Shah, A. Arai, S. Eaton, and P. Herman, "Waveguide writing in fused silica with a femtosecond fiber laser at 522 nm and 1 MHz repetition rate," Opt. Express **13**, 1999–2006 (2005).
56. T. Kondo, S. Juodkazis, and H. Misawa, "Reduction of capillary force for high-aspect ratio nanofabrication," Appl. Phys. A **81**, 1583 – 1586 (2005).

1. Introduction

Three-dimensional (3D) laser structuring of materials is widely used in photopolymer prototyping applications encompassing fields of photonic crystals (PhCs), micro-optical elements, parts of optically actuated micro-machines in microfluidics, scaffolds for cell growth, templates for plasmonic and meta-materials [1–5]. In order to achieve resolution of structuring required for PhCs operational at visible spectral range and for plasmonic applications, the feature sizes of 3D structures should become smaller or comparable with $\sim$100 nm in all cross sections. For this aim optical means of light beam delivery as well as material response should be precisely engineered [6–8]. In the case of 3D direct laser write both of these directions of a resolution

#125161 - $15.00 USD Received 8 Mar 2010; revised 2 Apr 2010; accepted 5 Apr 2010; published 30 Apr 2010

improvement are in their initial stages of development if we compare with sophistication of phase masks and materials used in planar semiconductor lithography [9].

The most popular materials in 3D laser photo-polymerization are acrylate and epoxy based resins and resists developed for one-photon stereolithography decades ago before the era of tabletop femtosecond lasers. Those photo-polymers are photo-sensitized for wavelength of eximer laser at 308 nm or i-line of Hg-lamp at 365 nm. Photo-sensitization and initiation of polymerization by an one-photon absorption is fundamentally different by its nature from a nonlinear photo-polymerization in the case of ultra-short laser pulses at longer wavelengths. Excitation of electronic subsystem occurs faster than an uptake of energy into ionic subsystem when ultra-short (sub-1 ps) laser pulses are used with subsequent electron-ion equilibration, recombination, and thermal diffusion. This energy relaxation facilitates chemical modifications of materials via combined thermal and photo-chemical pathways and can be well-controlled when fs-laser pulses with tens-of-megahertz repetition rate are used [10–16]. Better understanding of the photo-physical and chemical mechanisms of polymerization is still required [17–19] via quantitative measurements of nonlinear response of resists [20, 21]. Such studies would allow to optimize photo-polymers by tailoring their composition and chemical enhancement for the required resolution or sensitivity in 3D structuring applications.

Here, we demonstrate how a choice of photo-initiator and its concentration defines the achievable 3D resolution in direct laser writing by femtosecond laser pulses. It is shown that avalanche ionization plays an important part in photo-polymerization at tight focusing conditions even though a seeding stage of bond breaking and radical generation occurs via a nonlinear two-photon absorption (TPA). Resolution of 3D structuring at different formulations of photo-polymers followed prediction of two-photon nonlinearities [22], i.e., when TPA becomes stronger resolution worsens due to an enhanced polymerization rate. However, in the TPA photo-sensitized resists there is a wider processing window where high-quality and fidelity 3D structures can be prototyped.

2. Samples and methods

We use a hybrid sol-gel based resist SZ2080 [23] for photo-polymerization by direct laser writing. This resist consists of 20% of zirconia and 80% of polymer forming methacryloxypropyltrimethoxysilane (MAPTMS, Polysciences Inc.) and methacrylic acid (MAA, Sigma-Aldrich) both having photo-polymerizable methacrylate moieties [24] with different photoinitiators Irgacure 369 (2-Benzyl-2-dimethylamino-1-(4-morpholinophenyl)-butanone-1) and Michler's ketone (4,4'-bis(dimethylamino)benzophenone); referred to as Irg. and Bis., respectively. Detailed description of resist preparation is given in ref. [24]. Samples were prepared by drop-casting over a cover glass with subsequent annealing at 100°C for 1-2 h without a post-exposure bake.

The molecular density, which is used for estimation of bond breaking and radical generation can be calculated as $n_a = \rho N_a / M$, where N_a is the Avogadro number. It is difficult to estimate the molar mass of the resist, M, due to complex chemical modifications and evaporation of reaction products and solvents. For an order of magnitude estimation, let us consider amount of precursors: MAPTMS $M_{MAPTMS} \simeq 248$ g/mol, MAA $M_{MAA} \simeq 86$ g/mol, and zirconium npropoxide $Zr(OPr)_4$ zirconia, $M_{ZPO} = 328$ g/mol, at ratio 1:1:4, hence, $M_{SZ2080} \simeq 234$ g/mol; the mass density of resist used for calculations is assumed $\rho \simeq 1.2$ g/cm^3, typical for different photo-polymers. It is noteworthy that the precision in determination of n_a value was not critical for simulations and mechanisms discussed in Sec. 3.2; the actual value of n_a only slightly changes the moment of the breakdown at high irradiance during the laser pulse.

The photoluminescence excitation (PLE) spectra of the prepared films with and without photoinitiators are shown in Fig. 1 along with a typical cover glass substrate response. The influ-

#125161 - $15.00 USD Received 8 Mar 2010; revised 2 Apr 2010; accepted 5 Apr 2010; published 30 Apr 2010

ence of PL from the substrate for polymerization was negligible. After the laser structuring, the sample was developed in tetrahydrofuran or 4-methyl-2- pentanone and rinsed in isopropanol. 3D patterns recorded in the resist were analyzed by scanning electron microscopy (SEM) to determine feature size and integrity of 3D structures.

The 3D direct laser writing was carried out by tightly focused femtosecond (fs-)laser pulses at low 1 kHz repetition rate in order to avoid thermal accumulation. We used two different fs-lasers to compare fabrication at different wavelengths. The first fs-light source was a Ti:Sapphire laser Spitfire (Spectra Physics). The typical pulse energy for photo-polymerization at the dielectric breakdown conditions was ~ 5 nJ at the focal spot. An objective lens of numerical aperture $NA = 1.42$ was used to focus incoming laser pulses into a spot of approximately $2w = 1.22\lambda/NA$ diameter; the central laser wavelength was $\lambda = 800$ nm. The pulse duration was optimized by pre-chirping and was approximately 150 fs at the focus. An overlap between neighboring pulses was 50-100 nm required for recovery of 3D structures after development. It is noteworthy that the threshold for dielectric breakdown is 2.4 ± 0.2 nJ judged by a contrast change at the focal spot after one pulse irradiation, while the typical range of pulse energy used for 3D photonic crystal (PhC) fabrication is from 1.2 to 2.0 nJ when a weak or none of the optical contrast can be detected by an *in situ* observation during laser structuring.

The second fs-light source was a Yb:KGW solid-state laser Pharos (Light Conversion) operating at 1030 nm wavelength and delivering 300 fs pulses. The numerical aperture of an objective lens SPlanApo was $NA = 1.4$ and 100 nm spatial overlap of neighboring pulses (the corresponding scan speed is 100 μm/s). A spherical aberration due to refractive index mismatch between immersion oil ($n = 1.515$) and cover glass substrate is negligible and the depth of recording was just 10-20 μm to have aberration-free structuring conditions inside resists. The cross section of the focal volume has an axial extent larger than the lateral and depends on the *NA* value of the focusing optics. The ratio $axial/lateral$ was approximately 2.5-3.2 for the $NA = 1.3 - 1.4$ focusing. A typical feature size of polymerized structures closely follows this ratio as observed in the first photo-polymerized spirals [10] and logpile photonic crystals [12, 13, 25] in compliance with aberration and self-focusing free photo-polymerization.

We estimate the intensity considering the Gaussian spatial distribution at the focus $I(r) = \frac{2(E_p/t_p)}{\pi w^2}\exp(-2r^2/w^2)$ for pulse energy E_p and duration t_p. The equivalent intensity amplitude, $I_0 = \frac{2(E_p/t_p)}{\pi w^2}$, at the same average power can be approximated by a top-hat pulse of the radius $w_{TH} = \sqrt{2}w/2$ [26].

The dielectric breakdown threshold is defined by an ionization level corresponding to the critical plasma density, n_c, which is dependent on the wavelength of irradiation. The breakdown is conveniently recognized by visible spectrally broad plasma emission from the focal volume during laser structuring.

3. Theory

3.1. Role of nonlinear absorption and refraction

The most probable optically nonlinear effects occurring at the lowest irradiance/intensity are the two-photon absorption and refractive index changes via Kerr effect. The direct measurements of these nonlinear parameters are carried out by a Z-scan method [27] using ultra-short laser pulses, e.g., the best fit of an open aperture Z-scan data for the Gaussian spatial distribution of a laser pulse provides a measure of the TPA cross section. Other methods such as transmission measurements and photoluminescence are usually overestimating the actual TPA cross section [28, 29]. The intensity dependent TPA coefficient, β, and nonlinear refractive index, n_2, has been measured for many crystalline and amorphous materials [22, 30]. The same characteristic dependencies are also valid for molecular solutions of a highly efficient TPA absorber

#125161 - $15.00 USD Received 8 Mar 2010; revised 2 Apr 2010; accepted 5 Apr 2010; published 30 Apr 2010

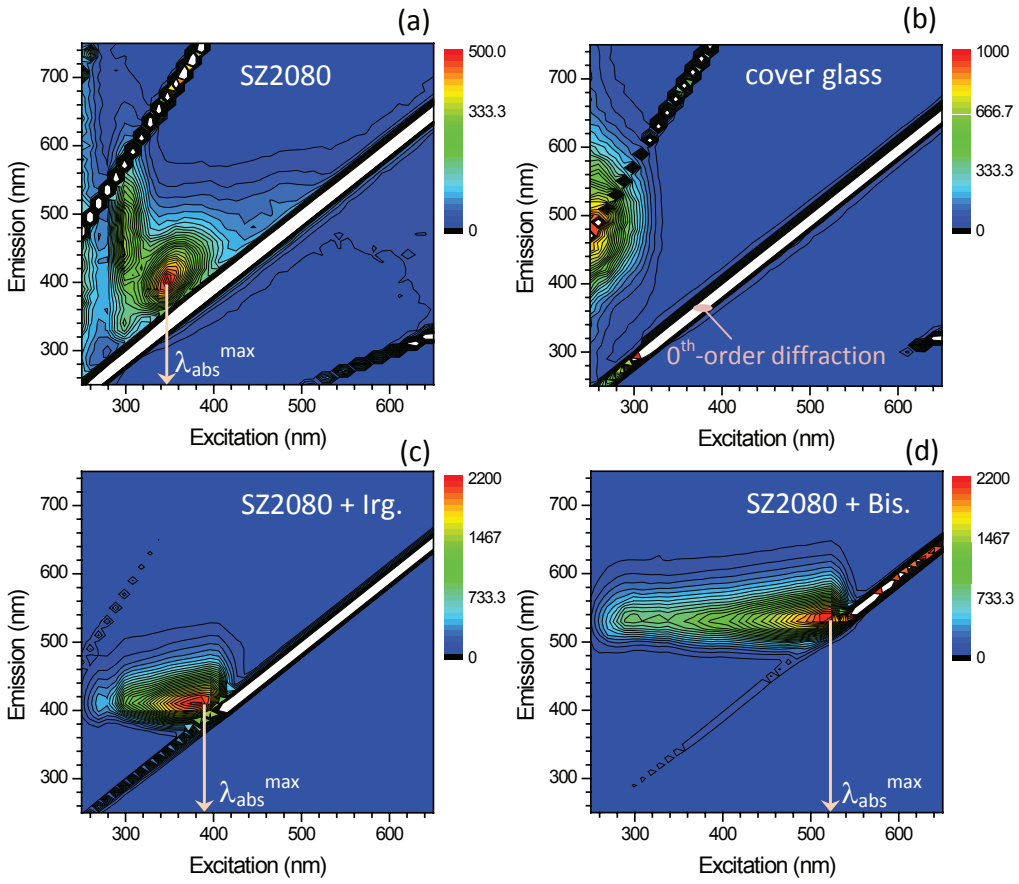

Fig. 1. The photoluminescence excitation (PLE) spectra of the pure resist SZ2080 (a), uncoated cover glass, resist with 2 wt% of Irgacure 369 (Irg.) and 4,4' - bis(diethylaminobenzo phenone) (Bis.) in (c) and (d), respectively. The wavelength of PLE maximum, λ_{abs}^{max}, corresponds to the most efficient in-bulk energy delivery required for the 3D structuring of chosen resists. Artifacts due to different orders of diffraction appear as slanted lines on the PLE maps; 0^{th}-order diffraction is marked in (b).

MBAPB [31] which is similar to photo-initiators used in resists [32, 33]. Optical nonlinearities of dyes and photo-initiators measured by fs Z-scan corroborated the expected spectral dependencies established in the case of inorganic solid-state materials [28].

The nonlinear refractive coefficient, n_2 $(n = n_0 + n_2 I)$ is given by [22, 30]:

$$n_2[cm^2/W] = K\frac{\hbar c\sqrt{E_p}}{2n_0^2 E_g^4} G_2(\hbar\omega/E_g) \tag{1}$$

where $E_p = 21$ eV, is an empirical constant, and G_2 is the universal function plotted in Fig. 2. The nonlinear TPA absorption coefficient, $\beta(\alpha = \alpha_0 + \beta I)$ is given by [22, 30]:

$$\beta[cm/W] = K\frac{\sqrt{E_p}}{n_0^2 E_g^3} F_2(2\hbar\omega/E_g) \tag{2}$$

where F_2 is the universal function plotted in Fig. 2. The G and F functions are defined by the following polynomial expressions: $G_2(x) = (2 + 6x - 3x^2 - x^3 - 3x^4/4 - 3x^5/4 + 2(1 -$

#125161 - $15.00 USD Received 8 Mar 2010; revised 2 Apr 2010; accepted 5 Apr 2010; published 30 Apr 2010

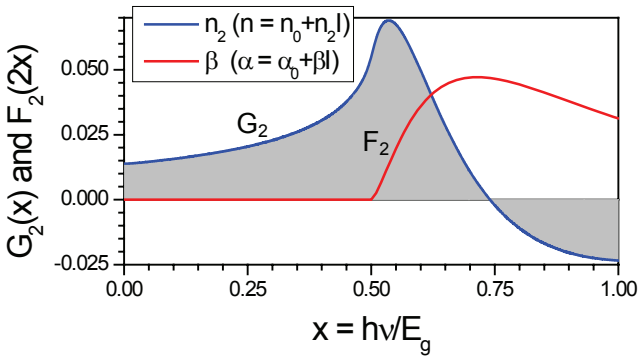

Fig. 2. Functional dependencies of the TPA coefficient, β, and nonlinear refractive index, n_2 on the normalized photon energy determined by the polynomial functions G_2 and F_2, respectively [22].

$2x)^{3/2}\Theta(1-2x))/(64x^4)$, here the Heaviside function $\Theta(y)=0$ for $y<0$ and $\Theta(y)=1$ for $y\geq 0$; $F_2(2x)=(2x-1)^{3/2}/(2x)^5$ for $2x>1$. Fig. 2 shows the functional dependencies for β and and n_2. The abscise value $x=1$ corresponds to the one-photon (or fundamental) absorption when photon energy is equal to the bandgap E_g. For our analysis, we use the corresponding λ_{abs}^{max} (Fig. 1) as the wavelength of the most efficient 3D structuring, i.e., it is strongly absorbed and, at the same time, the autofluorescence is strong. At this wavelength light can be in-bulk delivered and, if not absorbed, emission is reabsorbed promoting 3D polymerization. This wavelength defines the central wavelength of overlap between the absorption and emission spectra. For justification of a such wavelength choice corresponding to the $x=1$ condition, we tested the following procedure on MBAPB dye [33]. In case of MBAPB, the peak of PLE is $\lambda_{abs}^{max}=470$ nm and is considered corresponding to the bandgap wavelength (or $x=1$) while the strongest TPA has a plateau region at 680-710 nm. This is close to the expected location of the most efficient TPA [22, 30] (see, Fig. 2) at the 671 nm ($x=0.7$) in MBAPB. Hence, the choice of peak PLE at λ_{abs}^{max} for the photo-sensitizer is following expected spectral dependencies of two-photon nonlinearities (Eqs. (1)-(2)).

It may appear counter intuitive that at the half of the bandgap energy $x=0.5$ the TPA is not taking place (Fig. 2) [22]. Moreover, photons of half of bandgap energy experience the largest n_2, hence, self-focusing. However, this is consistent with a white light continuum generation which is related to the nonlinear refraction and is the most efficient when the photon energy of driving radiation is smaller than the half of bandgap.

In terms of 3D laser structuring the spectral dependence of the G and F functions would hint that a choice of irradiation wavelength for the most efficient photo-initiation of absorption is to be carefully chosen. The most optimal case for two-photon structuring is at the photon energy of $0.7E_g$ when β is the largest and n_2 is small. One can also recognize an expected tendency that closer to the fundamental absorption $(x=1)$ the n_2 values become negative as it would be expected due to free carrier absorption. Free carriers cause defocusing and alters light beam delivery to the focus. When linear absorption is present along with the nonlinear one, the refractive index changes per free electron, the dispersion volume, should be taken into account as well as the free carrier absorption. The procedures are well established by approaches in semiconductor physics. In solid state nomenclature, when band-to-band transitions are taking place simultaneously with the virtual ones (at $\hbar\omega<E_g$ as discussed above) the overall refractive index change can be described by [22]:

$$\Delta n = n_2 I + n_{e-h} N_c, \tag{3}$$

#125161 - $15.00 USD Received 8 Mar 2010; revised 2 Apr 2010; accepted 5 Apr 2010; published 30 Apr 2010

where N_c is the electron density in conduction band and n_{e-h} is the "dispersion volume" [34] [cm^3] or the change of the refractive index per one electron-hole pair, which can be estimated as $n_{e-h} = \frac{-e^2}{2n_0 m^* \varepsilon_0 \omega^2}$, where m^*, e are the effective electron mass and charge, respectively, and n_0 is the unperturbed refractive index.

3.2. *Rates of multi-photon and avalanche (impact) ionization*

The rates of multi-photon absorption and avalanche multiplication of electrons are estimated for the tight focusing and at the pre-breakdown conditions in photoresists. The number density of electrons n_e created to the end of the pulse together by avalanche and multi-photon processes can be obtained from a rate equation [35]:

$$\frac{dn_e}{dt} = n_e w_{imp} + n_a w_{mpi}, \tag{4}$$

where n_a denotes the molecular density, i.e., available electron donors after photo-cleavage of bonds (see, Sec. 2). If the laser intensity is constant during the laser pulse (corresponding to the top-hat intensity distribution) and when recombination during the pulse is negligible, a solution of Eq. (4) with the initial condition $n_e(t=0) = n_{e0}$ and w_{imp} and w_{mpi} is straightforward [35]:

$$n_e(I,\lambda,t) = \left\{ n_{e0} + \frac{n_a w_{mpi}}{w_{imp}} \left[1 - \exp(-w_{imp} t)\right] \right\} \exp(w_{imp} t). \tag{5}$$

It is commonly accepted that breakdown of a dielectric occurs when the plasma frequency of excited electrons equals to the frequency of laser light [36]. The critical electron density, the breakdown threshold, for 800 nm wavelength ($\omega = 2.35 \times 10^{15}$ s^{-1}) is $n_c = \frac{m_e \omega}{4\pi e^2} = 1.735 \times 10^{21}$ cm^{-3}.

Free electrons will oscillate in the electromagnetic field of the laser pulse. These electron can gain net energy by multiple electron-lattice/atom collisions and eventually be accelerated to reach the energy in excess of the ionization potential J_i. Energetic electrons create an avalanche which has the ionization rate estimated as follows [37]:

$$w_{imp} \approx \frac{\varepsilon_{osc}}{J_i} \frac{2\omega^2 \nu_{e-ph}}{\left(\nu_{e-ph}^2 + \omega^2\right)}, \tag{6}$$

here ν_{e-ph}, and ω are electron-phonon momentum exchange rate and laser frequency, respectively. Electron-phonon momentum exchange rate, the rate of collisions at the breakdown can be estimated as $\nu_{e-ph} = 6 \times 10^{14}$ 1/s [37]. The oscillation energy of electron in a scaling form reads [37]:

$$\varepsilon_{osc}[\mathrm{eV}] = 9.3 \left(\frac{I}{10^{14}\ [\mathrm{W/cm^2}]} \right) \lambda_{\mu m}^2, \tag{7}$$

which for 1 TW/cm^2 irradiance at 800 nm wavelength, yields $\varepsilon_{osc} = 30$ meV and is twice larger for a circularly polarized light.

The multi-photon ionization rate, a probability of ionization per atom per second, can be calculated according to [37]:

$$w_{mpi} \approx \omega n_{ph}^{3/2} \left(\frac{\varepsilon_{osc}}{2J_i} \right)^{n_{ph}}, \tag{8}$$

where n_{ph} is the integer part of $(J_i/\hbar\omega + 1)$ and defines the number of photons required for ionization [38]. The electron production rates via nonlinear two-photon absorption and avalanche will be estimated for the experimental conditions in the next section. This analysis is only

#125161 - $15.00 USD Received 8 Mar 2010; revised 2 Apr 2010; accepted 5 Apr 2010; published 30 Apr 2010

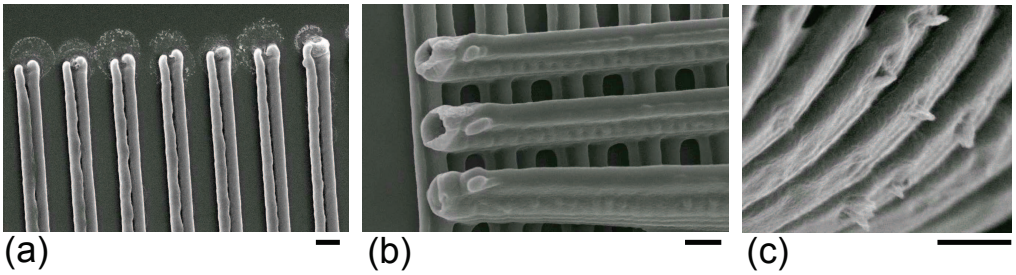

Fig. 3. SEM images of the first (a) and second (b) layer of 3D photo-polymerized logpile structures in SZ2080 resist with 2wt.% Irg. Polymerization was carried out by 800 nm/150 fs pulses of 5.2 nJ (at focal spot) focused by an objective lens of $NA = 1.42$ at the corresponding maximum intensity $I_0 = 18.7$ TW/cm^2. (c) Spiral recorded at 2 nJ or $I_0 = 7.2$ TW/cm^2. Scale bars, 1 μm.

valid as an order of magnitude estimate, however, it is insightful to determine the dominating mechanism of ionization, bond breaking, radical generation, and, hence, cross-linking and chain-polymerization.

4. Results

4.1. Photo-polymerization by dielectric breakdown at 800 nm

Light intensity threshold of dielectric breakdown in the case of single-pulse irradiation of SZ2080 with Irg. 2wt% by 150 fs pulses at 800 nm is ~ 8.6 TW/cm^2 (2.4 nJ per pulse at tight focusing). This intensity is comparable with the ionization threshold for the dielectrics [39].

The 3D laser structuring at the irradiance level of 5.2 nJ per pulse (approximately twice the dielectric breakdown threshold) was used for recording logpile patterns by 800 nm/150 fs pulses. Figure 3 shows close up views of the first and second layers of the logpile structure. A mid-split feature is recognizable in the first layer on the cover glass. The second layer of logpile structure is formed from hollow tubes rather than filled logs since laser irradiation was focused almost as in the bulk of resist. Both of these observations are consistent with dielectric breakdown and micro-explosion scenario. Ionization of material was high at the center of focal spot. It should be noted that self-focusing threshold of 1 - 3 MW per pulse typical in plastics and dielectrics has not been exceeded in these experiments (a pulse power was 0.2 MW). Hence, energy delivery to the focus was not perturbed by fillamentation. We can use simple estimations for the focal spot size given in Sec. 2. One can find that the irradiance per pulse was ~ 10 TW/cm^2. This is a typical irradiance for tight focusing at which the breakdown was observed in rubber- and glass-type polymers [40].

Figure 3(c) shows micro-explosion sites at the close-to-breakdown conditions. The needle-like protrusions on the surface of the 3D structure recorded at close to the dielectric breakdown threshold of 2 nJ are recognizable. Since pulses had slight power fluctuations such modifications occurred randomly. At the dielectric breakdown, the avalanche ionization becomes dominant in free electron generation and it is a linear process in terms of intensity [36]. These needle-like structures as well as hollow logs in polymerized structures are related to the avalanche and breakdown.

We calculate the multi-photon and impact ionization (avalanche) rates, w_{mpi}, w_{imp}, respectively, by formulas given in section Sec. 3.2. We consider the wavelength of absorption at PLE maximum (see, λ_{abs}^{max} in Fig. 1) $\lambda_{abs}^{max} \simeq 390$ nm (Irg. panel (c)) corresponding to the ionization potential $J_i[\mathrm{eV}] = 1.24/\lambda[\mu\mathrm{m}] \simeq 3.18$ eV. At the pulse energy equal to the breakdown

#125161 - $15.00 USD Received 8 Mar 2010; revised 2 Apr 2010; accepted 5 Apr 2010; published 30 Apr 2010

$E_p = 2.4$ nJ (at focus), the maximum intensity was 8.6 TW/cm^2 and $w_{mpi} = 0.81$ THz and $w_{imp} = 91.1$ THz. Hence, the avalanche generation of electrons is considerably more efficient than the multi-photon process though required for seeding the avalanche. The threshold pulse energy used for recording of 3D PhC structures was ~ 0.4 nJ or $I_0 = 1.4$ TW/cm^2 and $w_{mpi} = 0.0035$ THz and $w_{imp} = 14.8$ THz. The avalanche is even more dominant at the lower pulse energies. When the pulse energy is considerably higher than the breakdown threshold, the multi-photon rate catch up with the avalanche in electron generation and material experience breakdown on a very early stage of the laser pulse, a typical behavior in dielectrics [36]. The rest of pulse interacts with plasma and creates micro-explosion (see, Fig. 3). In all discussed 3D fs-laser fabrication conditions at tight focusing, the avalanche production of electrons via bond breaking is a dominant mechanism in radical generation which defines the rate of polymerization.

4.2. Photo-polymerization at 1030 nm

Figure 1 shows the PLE spectra of SZ2080 with different photo-sensitizers used in this study. In contrast to the SU8, where the auto-fluorescence is recognizable at wavelengths $\lambda_{abs}^{max} <$ 320 nm [41], the PLE peak is observed at $\lambda_{abs}^{max} \sim 340$ nm in a pure SZ2080 resist and at 390 and 520 nm in case of SZ2080 with Irg. and Bis. sensitizers, respectively (Fig. 1). For two-photon structuring at 800 nm wavelength the optimized resist is expected to have the λ_{abs}^{max} peak corresponding to the absorption wavelength of $1.24/(0.7 \times 3.1[\text{eV}]) = 571$ nm; for the 1030 nm laser irradiation the strongest TPA would occur around 736 nm (Fig. 2).

We used the 1030 nm wavelength, and a high $\sim 1-10$ TW/cm^2 irradiance to record 3D logpile structures. The w_{mpi} and w_{imp} rates slightly changes from those discussed above for 800 nm case, however, the condition $w_{imp} \gg w_{mpi}$ is even stronger fulfilled since the quiver energy of light-driven electrons scales as $\varepsilon_{osc} \propto \lambda^2$ (Eqn. 7).

Figure 4 shows the threshold resolutions achievable in 3D logpile recording in different resists. The smallest achievable width of 3D logpile structures are plotted in such a way (Fig. 4) that resists with different sensitization (λ_{abs}^{max}) structured at different wavelength λ_l can be compared with qualitative predictions of the two-photon absorption and refraction (the right axis). In order to recover fabricate 3D logpile structures in the case of all three different resists the concentration of photo-sensitizers was reduced to 1wt.%. In such case, the structures recorded in resists with photosensitizer were at the breakdown threshold similar to the one shown in Fig. 3(c), while in pure SZ2080 the very same condition corresponded to almost the threshold of 3D structuring (see, SEM insets in Fig. 4).

As resist gets more optimized for laser structuring by TPA (closer to $x = 0.7$), the feature sizes become larger. This is consistent with the analysis presented above: as seeding electrons are produced more efficiently and at the considerably higher avalanche rates as compared to multi-photon, the ionization becomes stronger facilitating polymerization via bond cleavage and thermal accumulation. A recognizable trend is that as λ_{abs}^{max} increases or/and λ_l decreases the smallest feature size increases even when TPA $\beta \to 0$ at $x \leq 0.5$. The smallest feature sizes can be obtained in a non-sensitized resist.

A qualitative comparison of fs-laser structuring regimes at 1030 nm/300 fs is given in Table 1 for 3D logpile structures in terms of pulse energy and irradiance at focus for the tight focusing with a $NA = 1.4$ objective lens. A narrow window of photo-structuring exist in the non-sensitized resist, however, the smallest feature sizes can be obtained in this case. Laser structuring of a more TPA sensitive material ($x \to 0.5$) results in larger feature sizes which are also more sensitive to laser power fluctuations and are prone to an uncontrolled spread of polymerization reducing resolution (e.g., see the inset (3) in Fig. 4).

#125161 - $15.00 USD Received 8 Mar 2010; revised 2 Apr 2010; accepted 5 Apr 2010; published 30 Apr 2010

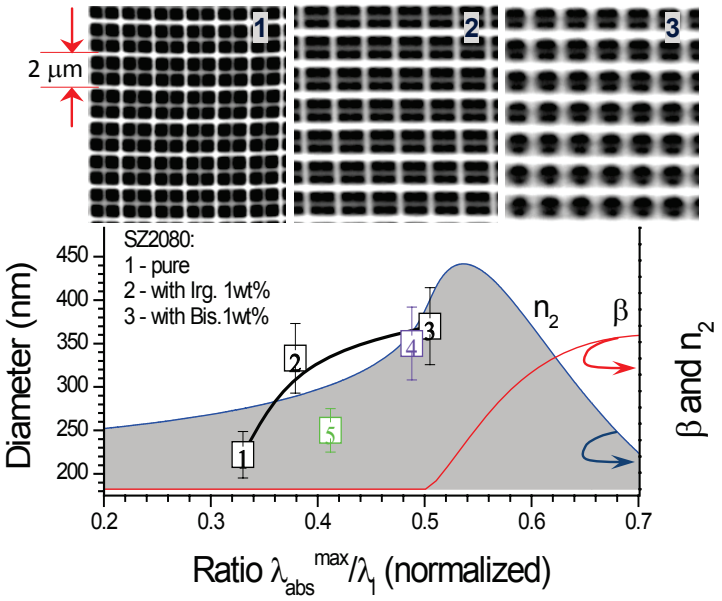

Fig. 4. The smallest width of a photo-polymerized log vs the ratio $\lambda_{abs}^{max}/\lambda_l$, where the λ_{abs}^{max} is the absorption maximum of the PLE (see, Fig. 1) and λ_l nm is the laser wavelength: 1030 nm *(1-3)* and 800 nm *(4,5)*. Right axis shows functional behavior of two-photon absorption, β, and refraction, n_2, (see, Fig. 2). Inset SEM images *(1-3)* show structures made at the same focusing conditions corresponding to: 13 TW/cm^2 at focus $I_0 = \frac{2(E_p/t_p)}{\pi w^2}$ for pulse duration of 300 fs, wavelength 1030 nm, pulse energy $E_p = 14.5$ nJ) in SZ2080 pure *(1)* and doped with 1 wt.% of Irg.*(2)* and Bis. *(3)*, respectively. The markers *(4,5)* corresponds to SZ2080 with 2 wt.% of Irg. and SU-8, respectively, structured with 800 nm, 150 fs pulses focused by $NA = 1.42$ objective lens and are shown here for comparison [42].

5. Discussion: photo-polymerization mechanisms at tight focusing and high irradiance

In practical use of photo-polymerization the quality of 3D structure, its resolution, mechanical and optical properties are the most important. By setting different pulse energies and scanning speeds the required window of photo-polymer processing is empirically found. Even a direct (i.e., one-photon) absorption can be used to obtain 3D micro-structures when tight focusing is employed [43, 44]. Let us discuss why so different resists and resins optimized for the one-photon absorption at the UV wavelengths still can be used for the 3D laser structuring at 800 and 1030 nm wavelengths using fs-laser sources. At those wavelengths TPA is usually negligible (Fig. 2).

Among important factors of the 3D laser structuring are laser repetition rate and overlap between laser pulses. The cooling time of the focal region can be estimated as the $t_c = d^2/D$, where d is diameter at focus approximately equal to the wavelength of irradiation at the tight focusing considered here; $D \simeq 10^{-3}$ cm^2/s is a typical thermal diffusion constant in polymers [45]. This yields in cooling time of $\sim 10\mu$s which is much longer than 12 ns between adjacent pulses in the case of 80 MHz repetition rate of fs-oscillators. Hence, the 3D laser structuring by oscillator irradiation is very different in terms of mechanism from that at few kHz repetition rate when the focal spot has time to cool down [46]. Here, we discuss a low repetition rate fabrication, which is the simplest case and was used in this study.

For the considered here case of the pre-breakdown and breakdown polymerization, the mech-

#125161 - $15.00 USD Received 8 Mar 2010; revised 2 Apr 2010; accepted 5 Apr 2010; published 30 Apr 2010

Table 1. Qualitative comparison of different laser structuring regimes for 1030 nm/300 fs pulses in SZ2080 at different photo-sensitization; focusing $NA = 1.4$ and scanning speed 100 μm/s.

Condition at focus, nJ (TW/cm^2):	SZ2080	SZ2080 + Irg.1wt%	SZ2080 + Bis.1wt%
Polymerization threshold	14 (12.5)	5 (4.5)	4 (3.6)
Quality structuring (middle of the range)	16 (14.4)	7 (6.3)	5 (4.5)
Explosion threshold (polymerized structure is recoverable)	17 (15.2)	12 (10.8)	12 (10.8)
Uncontrolled burning (no structure)	18 (16.1)	18 (16.1)	17 (15.2)

anism of electron generation, i.e., chemical bond breaking changes the effective photo-initiation pathways and the bond cleavage required for generation of radicals and cations can proceed directly via ionization of the host (in addition to the standard pathway via photo-initiator absorption and chemical bond opening). It has been established that unless pulse duration is less than approximately 10 fs, the avalanche (an impact ionization) is an efficient process fueled by multi-photon ionization [36]. This is confirmed here for the photo-polymers by the presented analysis (Sec. 4). It is also noteworthy that a standard role of photo-initiator (or a pair of photo-sensitizer with initiator) in providing free radicals (or cations) becomes different for a high-irradiance fs-pulse exposure. Once photo-initiator absorbed a photon and an electron in an excited state can undergo avalanche in a quasi-continuum of excited states and promote bond breaking, hence, polymerization. In a strongly ionized photo-polymer the avalanche is expected to be a prevalent mechanism in chemical bond cleavage as demonstrated by this order-of-magnitude estimation in Sec. 4. The avalanche usually proceeds with heating of the focal region since the kinetic energy of electron should exceed that of the bandgap by up to 50% in the case of fs-laser pulses in order to comply with energy and momentum conservation of the avalanche process [38].

It is noteworthy, that heat generated by exothermal photo-polymerization reaction is yet another factor enhancing polymerization. Since thermal polymerization of photo-polymers occurs at approximately 150°C, thermal accumulation can be used for a controlled heating of the focal volume providing a required control over 3D structuring [19]. Since polymerization and cross-linking depends exponentially on temperature this can provide an efficient method for 3D laser structuring of photo-polymers.

The threshold in 3D laser structuring appears as a result of cross-linking as it defines solubility of the resist during development and elastic properties of the final structure [47]. When a photo-polymerized structure is allowed to shrink freely in space during drying, the final size depends on the pulse energy exponentially [48]. Cross linking is temperature dependent and follows the Arrhenius mechanism, hence, the thermal effects are very efficient in photo-polymerization. In the case of tight focusing, the strong light intensity gradients create strongly localized thermal fields. Hence, a 3D structuring of resins and resists is possible even at the wavelengths close to the direct absorption band as was demonstrated by 355 nm 20 ps pulses in the acrylic resins [44].

The discussed mechanisms of electronic excitation (Sec. 4) are generic in dielectrics and semiconductors. Similar interplay between multi-photon and avalanche ionization takes place in the case of waveguide and microfluidic channel recording in glasses and crystals [49–55]. The electron generation rate can be estimated by the proposed approach and related to the processing window for the best performance of recorded structures.

Experimental data and presented analysis would suggest the following strategy for improve-

#125161 - $15.00 USD Received 8 Mar 2010; revised 2 Apr 2010; accepted 5 Apr 2010; published 30 Apr 2010

ment of resolution of 3D laser structuring. Shorter wavelengths of irradiation should be avoided, despite better focusing, due to more efficient seeding of electrons which ignites avalanche and polymerized structures have larger feature size (see, inset (3) in Fig. 4). Better resolution can be achieved by using photo-polymers with shorter PLE maxima, using longer wavelength of irradiation, having more pure and crystalline-like materials (with lesser probability of electronic excitation from Urbach states typical for amorphous materials). The described strategy corresponds to the $x \to 0$ condition which shows improvement in resolution (Fig. 4). However, at the longer wavelengths larger intensity should be used (Table 1) and the photo-polymerization has narrower processing window. Hence, a critical point drying equipment is required to avoid capillary collapse [56] of tiny polymerized structures during the final steps of wet processing. A settle interplay between the linear and nonlinear mechanisms of electronic excitation can be estimated for the known absorption of material at the excitation wavelength and irradiance following formulae given in Sec. 3.2. In most of conditions of practical interest at tight focusing of 30-300 fs duration pulses, the rate of electron generation by avalanche is larger than that by two (and multi) photon absorption.

6. Conclusions

The mechanisms of 3D polymerization are analyzed via rate equations of linear and non-linear electron generation in photo-polymers. The analysis demonstrated that avalanche rate of electron generation (hence, a chemical bond cleavage) is larger than that caused by nonlinear absorption at the typical 3D structuring of photo-polymers. These predictions are well supported by experimental evidence of 3D structuring of sol-gel resists with different photo-sensitization. The nonlinear absorption acts as a seeding mechanism for electronic excitation. The presented analysis can explain earlier results of 3D polymerization in very different resins and resists processed at different wavelengths and pulse durations.

Experiments of 3D photo-polymerization is carried out in sol-gel resist by femtosecond laser pulses at tight focusing and at (pre-)breakdown conditions when avalanche is prevalent. The observed structural changes supports numerical simulations of avalanche and micro-explosion scenario at high irradiance.

The highest resolution of 3D structures has been experimentally achieved in a non photo-sensitized resist, however, the widest processing window is observed in photo-sensitized resists. The presented analysis helps to select the best wavelength for 3D structuring of photo-polymers. When fs-pulses at high irradiance are used, the avalanche ionization plays an important role in chemical bond breaking and promotes polymerization. By better understanding of the photo-physical and photo-chemical processes we can create new resist and resin materials where true nano-structuring with sub-100 nm resolution in all three dimensions can be achieved.

Acknowledgments

We are grateful for support by a Discovery Grant DP0988054 from Australian Research Council, the Grant-in-Aid from the Ministry of Education, Science, Sports, and Culture of Japan No. 19360322, and to Dr. Hideki Fujiwara and Prof. Keiji Sasaki for access to photo-luminescence setup. Discussions with Dr. Kenji Kamada on two-photon absorption are gratefully acknowledged.

#125161 - $15.00 USD Received 8 Mar 2010; revised 2 Apr 2010; accepted 5 Apr 2010; published 30 Apr 2010